

Intrinsic alignments of galaxies and their effects on weak lensing detections of mass concentrations

Z.-H. Fan

Department of Astronomy, Peking University, Beijing 100871, China

fan@bac.pku.edu.cn

ABSTRACT

In this paper we investigate the influence of the intrinsic alignment of background galaxies on weak lensing detections of mass concentrations. Specifically, we analyze the number counts of false peaks resulting from intrinsic ellipticities in lensing convergence maps. Including the alignment of source galaxies, the full noise variance from intrinsic ellipticities in convergence κ -maps can be written as $\sigma_0^2 = \sigma_{0ran}^2 + \sigma_{0corr}^2$, where σ_{0ran}^2 is the noise contributed from randomly oriented source galaxies and σ_{0corr}^2 denotes the additional noise from intrinsic alignments. However, it is observationally difficult to measure σ_{0corr}^2 and usually only σ_{0ran}^2 can be estimated in weak lensing observations. Thus the observational signal-to-noise ratio is often defined with respect to σ_{0ran} , which is denoted as ν_{ran} in this paper. The true signal-to-noise ratio ν in terms of σ_0 is then $\nu = \nu_{ran} / (1 + \sigma_{0corr}^2 / \sigma_{0ran}^2)^{1/2}$. Given a detection threshold on ν_{ran} , a larger value of $\sigma_{0corr}^2 / \sigma_{0ran}^2$ leads to a lower threshold on ν and therefore a larger expected number of false peaks. With $\sigma_{0corr}^2 / \sigma_{0ran}^2 \sim 10\%$, the average number of false peaks with $\nu_{ran} \geq 3.5$ nearly doubles compared to that without considering the alignment, and for $\nu_{ran} \geq 5$, the number is tripled. As a result, the efficiency of weak lensing cluster detection degrades significantly. The increase of the number of false peaks also affects the likelihood of the existence of dark clumps. On the other hand, if one can observationally distinguish false peaks and peaks associated with real mass concentrations, e.g., using lensing tomography and follow up observations, the number of false peaks can be used to constrain tightly the level of intrinsic alignments of source galaxies. The CFHTLS Deep 3.61 deg² lensing observations and follow up studies find that 5 out of the 14 peaks with $\nu_{ran} > 3.5$ are likely to be false peaks, giving rise to a constraint $\sigma_{0corr}^2 \leq 1.6 \times 10^{-5} (1\sigma)$ at the angular scale of 1 arcmin for galaxies at redshift $z \sim 1$. This corresponds to $C_{11} + C_{22} \leq 3.2 \times 10^{-5}$, where C_{11} and C_{22} are, respectively, the angular correlations of intrinsic ellipticities e_1 and e_2 of background galaxies. This result is fully consistent with the limits on the intrinsic alignment derived directly from observations of Sloan Digital Sky Survey.

Subject headings: cosmology: theory — dark matter — galaxy: cluster — general
— gravitational lensing — large-scale structure of universe

1. Introduction

Gravitational lensing effects are the only ways to directly measure the distribution of dark matter in the universe (e.g., Hoekstra et al. 2006). Because of their dependence on the formation of structures as well as on the geometry of the universe, lensing effects are sensitive to the nature of dark energy, and therefore are highly promising in dark energy studies (e.g., Knox et al. 2006; Munshi et al. 2006). Weak gravitational lensing effects are mostly extracted from image distortions of background galaxies (e.g., Bartelmann & Schneider 2001). The intrinsic ellipticities of galaxies therefore present themselves as important errors in lensing observations (e.g., Kaiser & Squires 1993; Schneider 1996). It has been commonly assumed that the intrinsic ellipticities of different background galaxies are statistically uncorrelated, and thus the average shear measured over a large enough number of galaxies gives an unbiased estimate on the lensing effects (e.g., Kaiser & Squires 1993). However, the formation of galaxies is highly affected by their environment, and the shapes of galaxies can well be correlated if they are close enough. With the assumption that the shapes of galaxies are well represented by the shapes of their host dark matter halos, numerical simulations indicate that the shape correlations range from 10^{-5} to 10^{-3} on angular scales of a few arcminutes depending on halos masses and redshift distributions of source galaxies (e.g., Heavens et al. 2000; Croft & Metzler 2000; Jing 2002; Porciani et al. 2002; Heymans et al. 2006). The existence of such correlations can contaminate lensing signals significantly. Weak lensing effects are directly related to lensing potentials, and thus only the gradient modes, i.e., E -modes, are expected (e.g., Crittenden et al. 2001). The presence of B -modes can therefore be used to reveal the existence of different systematics including the intrinsic alignments, but the correction to the E -mode amplitude cannot be done in a straightforward way (e.g., Heymans et al. 2004). Down-weighting or removing physically closed pairs of background galaxies in lensing analyses reduces the contamination of intrinsic alignments at the expense of increasing shot noises if the alignments extend to relatively large scales (e.g., Heymans et al. 2004). Because of the different redshift-dependence for lensing signals and for intrinsic alignments, the tomographic method based on template fitting has been proposed to isolate different components assuming the availability of photometric redshifts for background galaxies (King & Schneider 2003). This method has also been extended to include shear-ellipticity cross correlations in the analyses (e.g., Hirata & Seljak 2004; King 2006).

The intrinsic alignments of galaxies have been searched observationally. The SuperCOSMOS data on nearby galaxies (with median redshift $z \sim 0.1$) reveal a level of 10^{-5} to 10^{-4} on the correlation of intrinsic ellipticities of galaxies over the angular scales of a few tens of arcminutes (Brown et al. 2002). Analyses on close pairs of galaxies from COMBO-17 data (with $z \sim 0.6$) find the intrinsic alignments to be consistent with zero but with uncertainties on the order of *a few* $\times 10^{-4}$ on scales of a few arcminutes (Heymans et al. 2004). Investigations on SDSS main sample with $z \sim 0.1$ and its subsamples with $z \sim 0.07$ to $z \sim 0.21$ conclude that no significant intrinsic alignments are detected (Mandelbaum et al. 2006). The observational results on the intrinsic alignments are close to the lower limits given by different numerical simulations on dark matter halos (e.g., Heymans et al. 2006). It has been pointed out that the existence of misalignment between baryonic matter and dark matter can significantly reduce the intrinsic alignment of background galaxies in comparison with that of dark matter halos and may explain the low observational results found in different surveys (Heymans et al. 2006).

In this paper, we study the effects of the intrinsic alignment on finding mass concentrations through weak lensing effects. Being the largest virialized objects in the universe, clusters of galaxies are important cosmological probes because their formation and evolution depend sensitively on cosmologies (e.g., Borgani 2006; Fan & Chiueth 2001). However, large uncertainties exist in linking cluster observables, such as galaxy richness, X-ray brightness and Sunyaev-Zeldovich effect, to their mass, the important quantity in cosmological analyses (e.g., Bode et al. 2006). On the other hand, lensing effects are generated through gravitation, and depend on the total mass distribution. Thus it is expected that a cluster sample detected through weak lensing effects is better suited for cosmological studies in comparison with those selected by other probes (e.g., White et al. 2002; Hamana et al. 2004; Tang & Fan 2005; Fang & Haiman 2006). Without involving complicated gas physics, weak lensing cluster detections, however, have their own shortcomings. Besides observational errors, physical systematics, such as projection effects and complex mass distributions of clusters of galaxies, affect the selection function of weak lensing clusters considerably. Thus weak lensing cluster samples are not truly mass-selected (Tang & Fan 2005). The intrinsic ellipticities of background galaxies result false peaks in lensing maps and reduce the efficiency of cluster detections significantly (e.g., White et al. 2002). The false peaks could also be misinterpreted as dark clumps, which might lead to a faulty conclusion regarding the validity of a cosmological model. Here we explore how the existence of the intrinsic alignment of background galaxies affects the number of false peaks in lensing convergence maps. We further propose that the number of false peaks can be used to constrain sensitively the level of the intrinsic alignment if one can separate true and false peaks observationally.

The rest of the paper is organized as follows. In §2, we discuss the correlations of galaxy

ellipticities based on the model proposed by Heymans et al. (2004; Heymans et al. 2006). In §3, we study the dependence of the number of false peaks on the intrinsic alignment of background galaxies. In §4, we analyze the constraints on the intrinsic alignment from the results of CFHTLS Deep on the number of false peaks given by Gavazzi and Soucail (2007). Discussions are presented in §5.

2. Intrinsic alignments of galaxies

Galaxies do not form in isolated ways. Environmental effects play important roles in shaping galaxies. Therefore correlations of ellipticities of galaxies are expected if they are close enough.

The ellipticity of a galaxy is defined through the second moments of its surface brightness profile $S(x, y)$. Specifically, we adopt the following definitions

$$2e_1 = \frac{I_{xx} - I_{yy}}{I_{xx} + I_{yy}}, \quad 2e_2 = \frac{2I_{xy}}{I_{xx} + I_{yy}}, \quad (1)$$

where (I_{yy} and I_{xy} have similar forms)

$$I_{xx} = \frac{\int S(x, y)(x_i - \bar{x})(x_i - \bar{x})dxdy}{\int S(x, y)dxdy}. \quad (2)$$

Here (\bar{x}, \bar{y}) are the coordinates of the center of the galaxy image. Concerning two-point correlations $c_{ij}(\vec{r}) = \langle e_i(\vec{x})e_j(\vec{x} + \vec{r}) \rangle$, it is convenient to choose x -axis and y -axis to be parallel and perpendicular to the line joining the two considered galaxies in the projected plane.

Numerical simulations show that $c_{12} = \langle e_1(\vec{x})e_2(\vec{x} + \vec{r}) \rangle \approx 0$ (e.g., Jing 2002; Heymans et al. 2004; Heymans et al. 2006). For $c_{ii} = \langle e_i(\vec{x})e_i(\vec{x} + \vec{r}) \rangle$ ($i = 1, 2$), we use the fitting formula provided by Heymans et al. (2004), which is

$$c_{ii} = \frac{0.001A_i}{1 + (r/B_i)^2}. \quad (3)$$

Our following analyses primarily concern $\eta(r) = \langle e_1(\vec{x})e_1(\vec{x} + \vec{r}) \rangle + \langle e_2(\vec{x})e_2(\vec{x} + \vec{r}) \rangle = c_{11} + c_{22}$, which can also be written as

$$\eta(r) = \frac{0.001A}{1 + (r/B)^2}. \quad (4)$$

Incorporating different galaxy models in numerical simulations, the fitting values of A and B are obtained for each model by Heymans et al. (2004; Heymans et al. 2006). Comparing

with SDSS observations, Mandelbaum et al. (2006) present their fitting results with $B = 1h^{-1}\text{Mpc}$, and $A = 0.57 \pm 0.72$ (see also Heymans et al. 2006).

To investigate their influence on weak lensing effects, we need to analyze the angular correlation of intrinsic ellipticities, which is related to the three dimensional correlation $c_{ij}(\vec{r})$ through the following equation

$$C_{ij}(\theta) = \frac{\int r_1^2 \phi(r_1) r_2^2 \phi(r_2) dr_1 dr_2 [1 + \xi(r_{12})] c_{ij}(r_p, \pi)}{\int r_1^2 \phi(r_1) r_2^2 \phi(r_2) dr_1 dr_2 [1 + \xi(r_{12})]}, \quad (5)$$

where $\phi(r)$ and $\xi(r)$ are the selection function and the two-point correlation function for background galaxies, and r_p and π are the comoving separations of two galaxies perpendicular and along the line of sight, respectively. Since the correlations decrease quickly on large scales, in the small-angle limit we have (e.g., Jing 2002),

$$C_{ij}(\theta) = \frac{\int r^4 \phi(r)^2 dr \Sigma_{ij}(r\theta)}{[\int r^2 \phi(r) dr]^2 + \int r^4 \phi(r)^2 dr \int d\pi \xi(r\theta, \pi)}, \quad (6)$$

where

$$\Sigma_{ij}(r_p) = \int d\pi [1 + \xi(r_p, \pi)] c_{ij}(r_p, \pi). \quad (7)$$

For weak lensing effects, both the convergence κ and the shear γ are determined by the second derivatives of the lensing potential ϕ , and

$$\kappa = \frac{\nabla^2 \phi}{2}, \quad \gamma_1 = \frac{(\phi_{,11} - \phi_{,22})}{2}, \quad \gamma_2 = \phi_{,12}, \quad (8)$$

where $\phi_{,ij} = \partial_i \partial_j \phi$.

Concerning weak lensing detections of mass concentrations, we focus on the convergence κ field. In the weak lensing limit, it is related to the shear γ in Fourier space through

$$\tilde{\kappa}(\vec{k}) = c_\alpha(k) \tilde{\gamma}_\alpha(\vec{k}), \quad (9)$$

where the summation over $\alpha = (1, 2)$ is implied, and $c_\alpha = [\cos(2\varphi), \sin(2\varphi)]$ with $\vec{k} = k(\cos \varphi, \sin \varphi)$ (Kaiser & Squires 1993). Observationally, the shear γ can be estimated from the ellipticities of galaxy images. In the weak lensing limit, we have

$$\mathbf{e}^{(O)} \approx \gamma + \mathbf{e}^{(S)}, \quad (10)$$

where \mathbf{e} is defined in eq.(1), and the superscripts 'O' and 'S' denote observed image and source, respectively. Then the noisy convergence κ_n including the contamination from source ellipticities follows

$$\tilde{\kappa}_n(\vec{k}) = c_\alpha(k) [\tilde{e}_\alpha^{(O)}(\vec{k})] = \tilde{\kappa}(\vec{k}) + c_\alpha(k) [\tilde{e}_\alpha^{(S)}(\vec{k})]. \quad (11)$$

Considering smoothed quantities, we have (e.g., van Waerbeke 2000)

$$\Sigma^{(O)}(\vec{\theta}) = \Gamma(\vec{\theta}) + \frac{1}{n_g} \sum_{i=1}^{N_g} W(\vec{\theta} - \vec{\theta}_i) \mathbf{e}^{(S)}(\vec{\theta}_i), \quad (12)$$

and

$$K_N(\vec{\theta}) = \int d\vec{k} e^{-i\vec{k} \cdot \vec{\theta}} c_\alpha(k) \tilde{\Sigma}_\alpha^{(O)}(\vec{k}), \quad (13)$$

where $\Sigma^{(O)}$, Γ , and $K_N(\vec{\theta})$ are the smoothed $\mathbf{e}^{(O)}$, γ and κ_n , respectively, $W(\vec{\theta})$ is the smoothing function, and n_g and N_g are, respectively, the surface number density and the number of source galaxies in the field. The noise part of K_N due to the intrinsic ellipticities is then

$$N(\vec{\theta}) = \frac{1}{n_g} \sum_{i=1}^{N_g} \int d\vec{k} \tilde{W}(\vec{k}) e^{-i\vec{k} \cdot (\vec{\theta} - \vec{\theta}_i)} c_\alpha(k) e_\alpha^{(S)}(\vec{\theta}_i), \quad (14)$$

where $\tilde{W}(\vec{k})$ is the Fourier transformation of the smoothing function with the form

$$\tilde{W}(\vec{k}) = \frac{1}{(2\pi)^2} \int d\vec{\theta} e^{i\vec{k} \cdot \vec{\theta}} W(\vec{\theta}). \quad (15)$$

Following van Waerbeke (2000), the correlation of $N(\vec{\theta})$ is calculated by averaging over both the ellipticities and the positions of source galaxies. Without intrinsic alignments, the correlation of $N(\vec{\theta})$ arises only from the smoothing operations, and by ignoring the non-uniform sampling of source galaxies, we have (van Waerbeke 2000)

$$\langle N(\vec{\theta}) N(\vec{\theta}') \rangle = \frac{\sigma_\epsilon^2}{2n_g} (2\pi)^2 \int d\vec{k} e^{i\vec{k} \cdot (\vec{\theta}' - \vec{\theta})} |\tilde{W}(\vec{k})|^2, \quad (16)$$

where σ_ϵ is the intrinsic dispersion of $\mathbf{e}^{(S)}$, and the factor $(2\pi)^2$ comes in to be in accord with the definition of $\tilde{W}(\vec{k})$ in eq. (15).

Including the alignment, the operation by averaging over the ellipticities of source galaxies, denoted by A following van Waerbeke (2000), is

$$A[e_\alpha^{(S)}(\vec{\theta}_i) e_\beta^{(S)}(\vec{\theta}_j)] = \frac{\sigma_\epsilon^2}{2} \delta_{\alpha\beta} \delta(\vec{\theta}_i - \vec{\theta}_j) + \delta_{\alpha\beta} C_{\alpha\beta}(\vec{\theta}_i - \vec{\theta}_j), \quad (17)$$

where $C_{\alpha\beta}(\vec{\theta}_i - \vec{\theta}_j)$ is given in eq. (6). Further by averaging over positions of galaxies, i.e., by applying the operation $(1/S^2) \int d\vec{\theta}_i d\vec{\theta}_j$ with S being the area of the field (van Waerbeke 2000), we get

$$\begin{aligned} \langle N(\vec{\theta}) N(\vec{\theta}') \rangle = & \frac{\sigma_\epsilon^2}{2n_g} (2\pi)^2 \int d\vec{k} e^{i\vec{k} \cdot (\vec{\theta}' - \vec{\theta})} |\tilde{W}(\vec{k})|^2 \\ & + (2\pi)^4 \int d\vec{k} e^{i\vec{k} \cdot (\vec{\theta}' - \vec{\theta})} |\tilde{W}(\vec{k})|^2 [c_1^2(k) \tilde{C}_{11}(\vec{k}) + c_2^2(k) \tilde{C}_{22}(\vec{k})], \end{aligned} \quad (18)$$

where $\tilde{C}_{11}(\vec{k})$ and $\tilde{C}_{22}(\vec{k})$ are the corresponding Fourier transformations of $C_{11}(\theta)$ and $C_{22}(\theta)$ discussed above. Thus the zero-lag noise variance can be written as $\sigma_0^2 = \sigma_{0ran}^2 + \sigma_{0corr}^2$, where

$$\sigma_{0ran}^2 = \frac{\sigma_\epsilon^2}{2n_g} (2\pi)^2 \int d\vec{k} |\tilde{W}(\vec{k})|^2, \quad (19)$$

and

$$\sigma_{0corr}^2 = (2\pi)^4 \int d\vec{k} |\tilde{W}(\vec{k})|^2 \frac{1}{2} [\tilde{C}_{11}(\vec{k}) + \tilde{C}_{22}(\vec{k})], \quad (20)$$

where the factor 1/2 is from the integration of $c_1^2(k) = \cos^2(2\phi)$ [and $c_2^2(k) = \sin^2(2\phi)$] over ϕ .

Considering Gaussian smoothings with

$$W(\theta) = \frac{1}{\pi\theta_G^2} \exp\left(-\frac{\theta^2}{\theta_G^2}\right), \quad (21)$$

where θ_G is the angular smoothing scale, we have

$$\sigma_{0ran}^2 = \frac{\sigma_\epsilon^2}{2} \frac{1}{2\pi\theta_G^2 n_g}, \quad (22)$$

and

$$\sigma_{0corr}^2 = \frac{1}{2\pi} \int d\vec{\theta} \frac{1}{2} [C_{11}(\theta) + C_{22}(\theta)] \frac{1}{\theta_G^2} \exp\left(-\frac{\theta^2}{2\theta_G^2}\right). \quad (23)$$

In the following analyses, we use eq. (4), (6) and (7) to calculate $C_{11}(\theta) + C_{22}(\theta)$, and further σ_{0corr}^2 from eq. (23).

The angular correlations $C_{ij}(\theta)$ depend sensitively on the redshift distribution of background galaxies. For galaxies distributed in a narrow range around a relatively low redshift, a large fraction of them are physically close to each other, resulting large $C_{ij}(\theta)$. We adopt the following functional form to describe the distribution of background galaxies

$$p(z) = \frac{\beta}{\Gamma[(1+\alpha)/\beta]} \left(\frac{z}{z_s}\right)^\alpha \exp\left[-\left(\frac{z}{z_s}\right)^\beta\right], \quad (24)$$

where α, β and z_s are parameters that can be determined from survey conditions. We take $\alpha = 2$ and $z_s = 0.7$. To see the effect of the width of the distribution, we vary the β value with $\beta = 1, 1.5, 3$, and 6. The larger the β value is, the narrower the distribution is, as seen in Figure 1. The corresponding median redshifts for the four distributions are $z_{med} \approx 1.87, 0.99, 0.62$ and 0.55 for $\beta = 1, 1.5, 3$, and 6, respectively.

In Figure 2, we show the results of σ_{0corr}^2 . For the intrinsic alignment, we take $A = 0.57$, the value from SDSS, in eq. (4) (e.g., Heymans et al. 2006). The solid, dotted, dashed,

and dash-dotted lines correspond to $\beta = 6, 3, 1.5$ and 1, respectively. For comparison, we also plot σ_{0ran}^2 (dash-dot-dot-dotted line) with $\sigma_\epsilon = 0.4$ and $n_g = 30 \text{ arcmin}^{-2}$. We see that the result with $\beta = 6$ and $z_{med} \sim 0.55$ is an order of magnitude larger than that with $\beta = 1$ and $z_{med} \sim 1.87$, demonstrating clearly the sensitive dependence of σ_{0corr} on the redshift distribution of background galaxies. Therefore for tomographic analyses of weak lensing effects with source galaxies distributed in narrow redshift bins, the effects of intrinsic alignments can be significant. The angular dependence of σ_{0corr}^2 is shallower than σ_{0ran}^2 , and the ratio of $\sigma_{0corr}^2/\sigma_{0ran}^2$ increases with the increase of smoothing scales.

In Table 1, we list $\sigma_{0corr}^2/\sigma_{0ran}^2$ for various cases. With the upper limit $A = 1.29$ from SDSS, the ratio can reach as high as about $\sigma_{0corr}^2/\sigma_{0ran}^2 \sim 20\%$ for $\beta = 6$ at $\theta_G = 2 \text{ arcmin}$. Notice that σ_{0ran}^2 and σ_{0corr}^2 depend differently on the distribution of source galaxies. While σ_{0corr}^2 depends mainly on the form of the redshift distribution, $\sigma_{0ran}^2 \propto n_g^{-1}$. Thus for surveys with higher surface number density of source galaxies than what we consider here, the ratio $\sigma_{0corr}^2/\sigma_{0ran}^2$ can increase considerably. Results expected for some surveys are presented in Table 2. The survey parameters for COSMOS are taken from Massey et al. (2007). For SNAP, we adopt the parameters used in Semboloni et al. (2007). For deep surveys with large n_g , tomographic analyses with source galaxies distributed in narrow redshift ranges become possible. For example, with total $n_g \sim 100 \text{ arcmin}^{-2}$ as expected from surveys similar to SNAP, the background galaxies can be divided into three bins each with $n_g \sim 30 \text{ arcmin}^{-2}$. The effect of intrinsic alignments can be significantly stronger within each bin than that in total. If we regard the narrow redshift distribution with $\beta = 6$ as one of the bins, it is seen from Table 1 that the respective values of $\sigma_{0corr}^2/\sigma_{0ran}^2$ for $\theta_G = 1$ and 2 arcmin are about 5% and 10% with $A = 0.57$, in comparison with 3.3% and 5% expected for the full sample of galaxies from SNAP as seen in Table 2.

In next section, we show that the number of false peaks in lensing κ -maps is very sensitive to the ratio of $\sigma_{0corr}^2/\sigma_{0ran}^2$. Even a relatively low value of σ_{0corr}^2 can result a considerable increase of the number of false peaks, and therefore reduce the efficiency of cluster detections significantly.

3. Statistics of false peaks in κ -maps resulting from intrinsic ellipticities

Weak lensing cluster detections associate high peaks in κ -maps reconstructed from shear measurements with clusters of galaxies. Intrinsic ellipticities of background galaxies can produce false peaks, and therefore affect the efficiency of cluster detections. It is thus important to understand the statistics of false peaks thoroughly in order to extract reliable cluster samples from weak lensing surveys. van Waerbeke (2000) studies the number of false peaks

assuming no intrinsic alignments for source galaxies. In this case, the smoothed quantity $N(\vec{\theta})$ defined in eq. (14) is approximately a Gaussian random field because of the central limit theorem. Including the correlations of the intrinsic ellipticities, the statistics of the noise field $N(\vec{\theta})$ can be complicated. Relating the intrinsic ellipticities linearly with the tidal field predicts Gaussian statistics. Assuming that they are associated with galaxy spins gives rise to non-Gaussian statistics for the intrinsic ellipticities. On the other hand, $N(\vec{\theta})$ is related to the sum of the intrinsic ellipticities of background galaxies in the smoothing window. Since the intrinsic alignments are relatively weak (on the order of 10^{-6} to 10^{-5} at $\theta_G \sim 1$ arcmin), according to the central limit theorem we do not expect a highly non-Gaussian field for $N(\vec{\theta})$ if the number of galaxies within the smoothing window is large enough. In our following analyses, we assume the Gaussianity for $N(\vec{\theta})$. Detailed studies on its statistics will be carried out in our future investigations.

For a two dimensional Gaussian random field N , the differential number density of peaks can be written explicitly in the following form (Bond & Efstathiou 1987; van Waerbeke 2000)

$$n_{peak}(\nu) = \frac{1}{2\pi\theta_*^2} \exp(-\nu^2/2) \frac{G(\gamma_p, \gamma_p\nu)}{\sqrt{2\pi}}, \quad (25)$$

where $\nu = N/\sigma_0$ is the significance of a peak with N being the value of the considered quantity at the peak position, $b = \sqrt{2(1 - \gamma_p^2)}$, and

$$\begin{aligned} G(\gamma_p, \hat{x}) &= \frac{1}{2} \left(\hat{x}^2 + \frac{b^2}{2} - 1 \right) \operatorname{erfc} \left(-\frac{\hat{x}}{b} \right) + \frac{\hat{x}b}{2\sqrt{\pi}} \exp(-\hat{x}^2/b^2) \\ &+ \frac{1}{2(1+b^2)^{1/2}} \exp[-\hat{x}^2/(1+b^2)] \operatorname{erfc} \left(-\frac{\hat{x}}{b\sqrt{1+b^2}} \right). \end{aligned} \quad (26)$$

It is seen that $n_{peak}(\nu)$ is fully characterized by γ_p and θ_* , which are respectively defined as

$$\gamma_p = \frac{\sigma_1^2}{\sigma_0\sigma_2} \quad \text{and} \quad \theta_* = \sqrt{2} \frac{\sigma_1}{\sigma_2}, \quad (27)$$

where

$$\sigma_n^2 = \int d\vec{k} \, k^{2n} < |N(k)|^2 >. \quad (28)$$

Considering the noise field $N(\theta)$ defined in eq. (14), with Gaussian smoothings we have $\gamma_p = \sqrt{2}/2$ and $\theta_* = \theta_G/\sqrt{2}$ in the case without intrinsic alignments (van Waerbeke 2000). Thus the average cumulative number density of peaks $N_{peak}(\nu_{ran}) = \int_{\nu_{ran}} n_{peak}(\nu') d\nu'$ is independent of σ_{0ran} and scales with the smoothing angle as θ_G^{-2} . In this case, given a survey area and a smoothing angle θ_G , the average number of false peaks in terms of the significance ν_{ran} is fixed regardless of the specific value of σ_{0ran} . Note that the existence of

false peaks is the result of chance alignments of background galaxies. Given $\nu_{ran} = N/\sigma_{0ran}$ for a false peak, its strength N is proportional to σ_{0ran} which is in turn determined by n_g and σ_ϵ . Thus the number of false peaks measured by their strength N depends on n_g and σ_ϵ . Smaller n_g or larger σ_ϵ gives rise to larger σ_{0ran} and leads to higher probabilities in forming false peaks with large N by chance alignments.

Including the intrinsic alignments, both γ_p and θ_* , and thus the number density of false peaks in terms of the true significance ν , depend on the correlation level. It is noted from Figure 2 that the level of intrinsic alignments from current observations is low comparing with σ_{0ran} . Therefore γ_p , θ_* , and $n_{peak}(\nu)$ change only slightly with respect to the case without intrinsic alignments.

The number of false peaks discussed above is given in terms of the true significance $\nu = N/\sigma_0$, i.e., the peak height is measured relative to the full noise variance $\sigma_0 = \sqrt{\sigma_{0ran}^2 + \sigma_{0corr}^2}$ including σ_{0corr} . Observationally however, it is difficult to obtain σ_{0corr} , and thus usually only σ_{0ran} is estimated and used in measuring the significance of a peak. The true significance of the peak corresponding to the observed significance $\nu_{ran} = N/\sigma_{0ran}$ is then $\nu = \nu_{ran}/(1 + \sigma_{0corr}^2/\sigma_{0ran}^2)^{1/2}$. Given a threshold on ν_{ran} , the average number of peaks is $N_{peak}(\nu_{ran}) \propto \int_\nu n_{peak}(\nu') d\nu'$. Because $\nu < \nu_{ran}$ for non-zero σ_{0corr} , N_{peak} increases with the increase of σ_{0corr} .

In Figure 3, we show $N_{peak} - N_{peak}^{ran}$, the number of false peaks resulting from intrinsic alignments, with respect to the detection threshold ν_{ran} , where N_{peak} and N_{peak}^{ran} are the cumulative numbers of false peaks in 1 deg^2 with and without intrinsic alignments. For comparison, we also plot N_{peak}^{ran} (thick lines) in each panel. The left and right panels are respectively for $\theta_G = 1 \text{ arcmin}$ and $\theta_G = 2 \text{ arcmin}$. The upper panels are for $A = 0.57$, and the lower panels are for $A = 1.29$. The thin solid, dotted, dashed, and dash-dotted lines in each panel are for $\beta = 6, 3, 1.5$ and 1 , respectively. It is seen that $N_{peak} - N_{peak}^{ran}$ can be comparable to N_{peak}^{ran} . For $\theta_G = 1 \text{ arcmin}$, $N_{peak}^{ran} \sim 2, 0.3, 0.04$, and 0.004 at $\nu_{ran} = 3.5, 4, 4.5$ and 5 , respectively. The corresponding $N_{peak} - N_{peak}^{ran}$ are $0.25, 0.06, 0.013$, and 0.0015 for $\beta = 1.5$ and $A = 1.29$. For larger β , the numbers are larger and $N_{peak} - N_{peak}^{ran} > N_{peak}^{ran}$ when $\nu_{ran} > 3.7$ and 4.5 for $\beta = 6$ and 3 , respectively. For $\theta_G = 2 \text{ arcmin}$, $N_{peak} - N_{peak}^{ran} > N_{peak}^{ran}$ when $\nu_{ran} > 3, 3.8$ and 5.3 for $\beta = 6, 3$ and 1.5 , respectively. Therefore the existence of intrinsic alignments can result significant number of extra false peaks in lensing convergence maps.

In Figure 4, we show the dependence of the ratio $r_{peak} = N_{peak}/N_{peak}^{ran}$ on the level of intrinsic alignments represented by the amplitude A for $\theta_G = 1 \text{ arcmin}$. The β value in each panel is written out explicitly. The solid, dotted, dashed and dash-dotted lines are respectively for $\nu_{ran} = 5, 4.5, 4$ and 3.5 . For $\beta = 1.5$ and $A = 1.29$, we have $r_{peak} \sim 1.36$,

1.27, 1.2 and 1.14 for $\nu_{ran} = 5, 4.5, 4$ and 3.5 , respectively. With larger smoothing scales, the relative effect of intrinsic alignments is higher. For $\theta_G = 2$ arcmin, the corresponding ratios change to 1.6, 1.4, 1.3 and 1.2. For $\beta = 6$, the ratios for $\nu_{ran} = 5$ reach as high as 3.8 and 7.6 for $\theta_G = 1$ and 2 arcmin, respectively.

From eqs. (25) and (26), it can be shown that N_{peak} depends largely on the detection threshold with $N_{peak} \propto \nu \exp(-\nu^2/2)$ at $\nu > 3$ (e.g., van Waerbeke 2000). Given a detection threshold on ν_{ran} , the corresponding threshold for the true significance is $\nu = \nu_{ran}/(1 + \sigma_{0corr}^2/\sigma_{0ran}^2)^{1/2}$, which decreases with the increase of $\sigma_{0corr}^2/\sigma_{0ran}^2$. Thus r_{peak} is largely determined by the ratio $\sigma_{0corr}^2/\sigma_{0ran}^2$. In Figure 5, we show r_{peak} with respect to $\sigma_{0corr}^2/\sigma_{0ran}^2$ for $\theta_G = 1$ (upper panel) and 2 arcmin (lower panel). The four sets of lines from top to bottom in each panel correspond respectively to the threshold $\nu_{ran} = 5, 4.5, 4$ and 3.5 . Note that each set contains four lines with $\beta = 6, 3, 1.5$, and 1 , respectively. With $\sigma_{0corr}^2/\sigma_{0ran}^2 \sim 5\%$, the values of r_{peak} are about 1.7, 1.55, 1.4 and 1.3 for $\nu_{ran} = 5, 4.5, 4$ and 3.5 . For $\sigma_{0corr}^2/\sigma_{0ran}^2 \sim 10\%$, the corresponding r_{peak} are 2.9, 2.3, 1.9 and 1.6. A specific value of $\sigma_{0corr}^2/\sigma_{0ran}^2$ depends on the strength of the intrinsic alignment, the surface number density and the redshift distribution of source galaxies, and σ_ϵ . The dotted vertical lines from left to right in each panel show the corresponding values of $\sigma_{0corr}^2/\sigma_{0ran}^2$ for $\beta = 1, 1.5, 3$ and 6 , where we take $A = 1.29$, $\sigma_\epsilon = 0.4$, and $n_g = 30 \text{ arcmin}^{-2}$. It should be noted that n_g usually varies with the redshift distribution of source galaxies. Surveys that can reach high redshifts typically have large n_g . Thus our estimates on $\sigma_{0corr}^2/\sigma_{0ran}^2$ with fixed $n_g = 30 \text{ arcmin}^{-2}$ may overestimate the ratio for $\beta = 6$. On the other hand, for deep surveys with large n_g (e.g., $n_g \sim 100$ for SNAP, and $n_g \sim 300$ for SNAP Deep), we can divide the source galaxies into different bins with $n_g \sim 30 \text{ arcmin}^{-2}$ in each bin. In this case, the narrow distribution with $\beta = 6$ can be one of these bins, and our above estimate on $\sigma_{0corr}^2/\sigma_{0ran}^2$ with $n_g = 30 \text{ arcmin}^{-2}$ can be a representative value for galaxies within the bin.

For weak lensing cluster surveys, the efficiency measures how efficient we can find true clusters from lensing maps. Assuming the NFW profile (Navarro, Frenk and White 1996) for the mass distribution of clusters of galaxies, it is found that the number of peaks resulting from true clusters in lensing κ -maps is about 6 deg^{-2} , and 4 deg^{-2} for significance larger than 3.5 and 4, respectively, where $\sigma_\epsilon = 0.4$, $n_g = 30 \text{ arcmin}^{-2}$ and $\theta_G = 1$ arcmin are used (Hamana et al. 2004). As we show previously, the corresponding N_{peak}^{ran} are about 2 and 0.3. Then a simple estimate gives the efficiency about 75% and 93% for the two detection thresholds if there are no intrinsic alignments. With $\sigma_{0corr}^2/\sigma_{0ran}^2 \sim 10\%$, the corresponding efficiencies drop to 65% and 87%. Note that we only consider the contamination from false peaks when estimating the above efficiencies. The existence of intrinsic ellipticities and alignments not only results false peaks but also affects the heights of true peaks, which can further decrease the efficiency of weak lensing cluster detections considerably (e.g., Hamana

et al. 2004).

Because weak lensing effects arise from the gravitational influence of the matter distribution, it is expected that dark clumps without luminous counterparts can be discovered from lensing observations. The existence of massive dark clumps would question the current theory of structure formation seriously. There have been such candidates reported in literature. Erben et al. (2000) present CFHT weak lensing results around the galaxy cluster Abell 1942. They find a high peak [$\sim 5\sigma$ in the aperture-mass measurement (Schneider 1996)] without associated galaxy overdensities at the location about $7'$ south of the main cluster. Faint X-ray emissions from the nearby region of the peak are detected by ROSAT, but they may not be related to the lensing peak signal. With HST lensing observations in this field, Linden et al. (2006) also find a peak at a place consistent with that given by Erben et al. (2000), but with a much lower significance $\sim 2.9\sigma$. Further, they divide the source galaxies into three magnitude bins and perform lensing analyses for each of them. For the bright bin, which contains most of the source galaxies used in Erben et al. (2000), they find a 1.9σ peak with a smoothing scale $120''$. For the faint bin, a 3.3σ peak is detected. There is no lensing detection from the medium bin, which is unexpected if there is a foreground dark clump. A spatial concentration of galaxies in the medium bin is observed, which could act as the lens for galaxies in the faint bin but not for those in the bright bin. The lack of lensing detections in the medium bin and the low significance of the peak from HST observations raise questions on the lensing origin of the peak. It is likely that the peak is a statistical fluke (Linden et al. 2006). On the other hand, Erben et al. (2000) estimate the probability that their detected peak is a false one from chance alignments of background galaxies. In order to apply the results given by van Waerbeke (2000), they perform a Gaussian smoothing with $\theta_G \approx 0.5'$ to the κ field, and find that the considered peak has a height of $\nu_{ran} \sim 4.5\sigma$. The probability to have such a high peak from chance alignments is very low (Erben et al. 2000).

Our analyses show that the existence of intrinsic alignments can increase the chance for the appearance of false peaks in a given area depending on the ratio of $\sigma_{0corr}^2/\sigma_{0ran}^2$. In Table 3, we list the probabilities that the detected 'dark clumps' are false peaks for different observations. The probability is calculated from the Poisson statistics with

$$p_n = \frac{e^{-N_{peak}} N_{peak}^n}{n!}, \quad (29)$$

where p_n is the probability to have n false peaks in a field, and N_{peak} is the average number of false peaks expected in the field. For the observation of Erben et al. (2000), we estimate $\sigma_{0corr}^2/\sigma_{0ran}^2 \sim 1.3\%$ (with $A = 1.29$) for $\theta_G = 0.5$ arcmin. With this level of intrinsic alignment, the probability to find one $\nu_{ran} = 4.5$ false peak in the field of $14' \times 14'$ increases only slightly from 0.9% to 1%. On the other hand, with the noise level comparable to that of Erben et al. (2000), the average surface number density of peaks with $\nu_{ran} \geq 4.5$ resulting

from the lensing effects of true mass concentrations is about 3 deg^{-2} for $\theta_G = 0.5 \text{ arcmin}$ (Hamana et al. 2004). Then the average number of true peaks in the field of $14' \times 14'$ is about 0.15, and the probability to have one true peak in this field is $\sim 13\%$. Thus the $\nu_{ran} = 4.5$ peak found by Erben et al. (2000) is much more likely to be associated with a true mass clump than being a false peak. However the analyses on HST data by Linden et al. (2006) give $\nu_{ran} \sim 3$ for the peak. The average number of false peaks expected in the field of $14' \times 14'$ with $\nu_{ran} \geq 3$ is about 1.7 with $\sigma_{0corr}^2 = 0$. For source galaxies in Linden et al. (2006), we estimate $\sigma_{0corr}^2/\sigma_{0ran}^2 \sim 5\%$ with $A = 1.29$. Then the average number of false peaks increases to ~ 2 , and the corresponding probability $p(corr) \sim 27\%$. In this case, it is quite possible that the observed peak is a false one. The reason for the difference between the peak heights from CFHT and HST is unclear (Linden et al. 2006), and so is the conclusion on the origin of the peak. It is likely that the peak is associated with a small mass clump and its height is enhanced by the chance alignment of background galaxies (Linden et al. 2006).

Massey et al. (2007) present the COSMOS 2 deg^2 lensing analysis. They notice the existence of two high peaks without luminous counterparts near the main cluster. The κ field in Massey et al. (2007) is reconstructed using the wavelet method and its noise properties are complicated (e.g., Starck, Pires, & Refregier 2006). The significances of the peaks are not clearly given in Massey et al. (2007). Thus in Table 3, we include the probabilities for different significances. When calculating $p(corr)$, we use $\sigma_{0corr}^2/\sigma_{0ran}^2 \sim 5\%$ estimated for the redshift distribution of source galaxies with $\alpha = 2$, $\beta = 1.5$ and $z_s = 0.8$. It is seen that with the intrinsic alignments, the probability that the two peaks are false ones is tripled for $\nu_{ran} > 5$. It is noted that our results are for Gaussian smoothings, and therefore cannot be used directly to discuss how likely the peaks found by Massey et al. (2007) are false ones. On the other hand, the COSMOS data can be readily analyzed with the method of Kaiser & Squires (1993) with Gaussian smoothings. Then our studies presented here can be directly applicable.

4. Constraints on intrinsic alignments from CFHTLS Deep survey

Because of its sensitive dependence on intrinsic alignments, the number of false peaks can be used to probe the strength of the intrinsic alignments of source galaxies if one can observationally distinguish false and true peaks. In this section, we analyze the constraints on σ_{0corr}^2 from the results of the CFHTLS Deep survey (Gavazzi & Soucail 2007).

The CFHTLS Deep survey shares the same data with the Supernova Legacy Survey (SNLS). It contains four independent fields and includes data from five bands (g', r', i', z', u^*).

The shear measurements are done using the i' band images with magnitude in the range $22 < i' < 26$. The seeing is $\sim 0.9''$. The total working area for weak lensing analysis is 3.61 deg^2 . The photometric redshift is estimated for each source galaxy with the multi-band observational data. The redshift distribution for a subsample of source galaxies with reliable photo- z measurements is presented in Figure 3 of Gavazzi & Soucail (2007), which will be used in our following analysis. The convergence κ -map is constructed from the inferred shear γ with the technique developed by Kaiser and Squires (1993). The shear and consequently the κ fields are smoothed with a Gaussian window function with $\theta_G = 1 \text{ arcmin}$. The variance of noise in the smoothed κ field from randomly oriented background galaxies is estimated to be $\sigma_{0ran} = 0.0196, 0.0225, 0.0202$, and 0.0221 for the four fields, respectively (Gavazzi & Soucail 2007). The signal-to-noise ratio ν is defined as $\nu_{ran} = \kappa/\sigma_{0ran}$. From the κ -maps of the four fields, Gavazzi and Soucail (2007) detect ~ 46 peaks with $\nu_{ran} > 3$, 14 peaks with $\nu_{ran} > 3.5$ and 5 peaks with $\nu_{ran} > 4$. Detailed studies are done for the 14 peaks with $\nu_{ran} > 3.5$. With the help of photometric redshift measurements, X-ray observations and the lensing tomographic analysis, they claim that there are 9 secure cluster detections among the 14 peaks. The rest 5 are likely false peaks. In our study here, we regard these 5 peaks as false ones resulting from the intrinsic ellipticities of background galaxies, and constrain the level of intrinsic alignments based on our analysis presented in the previous section. It is worth mentioning that the statistics based on only 5 peaks is poor, and therefore our analysis mainly aims at demonstrating the feasibility in extracting the information of the intrinsic alignments of background galaxies from the number of false peaks. Also some of the five peaks may result from dark clumps without luminous counterparts. Larger weak lensing cluster surveys with more reliable tomographic analyses will provide statistically meaningful results on the intrinsic alignments.

We model the redshift distribution shown in Gavazzi & Soucail (2007) as

$$p(z) \propto \left(\frac{z}{z_s}\right)^2 \exp\left[-\left(\frac{z}{z_s}\right)^2\right] + 0.07 \exp\left[-\frac{(z-2.8)^2}{0.6^2}\right], \quad (30)$$

where z_s is taken to be 0.8. The second term is added to describe the low bump at $z \sim 3$ seen in the redshift distribution of the source galaxies of CFHTLS Deep (Gavazzi & Soucail 2007). This term does not affect much our results because of its low amplitude. We calculate σ_{0corr} from eq.(23) with $\theta_G = 1 \text{ arcmin}$, where C_{11} and C_{22} are computed from eqs. (4)-(7).

In Figure 6, we show the dependence on $\sigma_{0corr}^2/\sigma_{0ran}^2$ of the expected number of false peaks detected in 3.61 deg^2 . The solid line is for the average number of false peaks. The upper and lower dashed lines show the -1σ and -2σ Poisson deviations from the mean, i.e., $N_{peak} - \sqrt{N_{peak}}$ and $N_{peak} - 2\sqrt{N_{peak}}$, respectively. The horizontal dash-dotted line is located at $N_{peak} = 5$. The vertical dotted lines indicate the values of $\sigma_{0corr}^2/\sigma_{0ran}^2$ for the

source galaxies of CFHTLS Deep with $A = 0.57$ and $A = 1.29$, from left to right, respectively. We see that 1σ and 2σ constraints give $\sigma_{0corr}^2/\sigma_{0ran}^2 < 4\%$ and $< 14\%$. With $\sigma_{0ran}^2 = 0.0004$, we have $\sigma_{0corr}^2 < 1.6 \times 10^{-5}$ and $\sigma_{0corr}^2 < 5.6 \times 10^{-5}$ for 1σ and 2σ constraints. From eq. (23), it is seen that $2\sigma_{0corr}^2$ corresponds to the intrinsic alignment $C_{11} + C_{22}$ smoothed over the angular scale θ_G . Thus we have the 1σ and 2σ constraints on $C_{11} + C_{22}$ for $\theta_G = 1$ arcmin to be $< 3.2 \times 10^{-5}$ and $< 1.1 \times 10^{-4}$. The corresponding limits on the amplitude of the intrinsic alignments A are $A < 2.9$ and $A < 10$. The results are fully consistent with that from SDSS observations with $A < 1.29$.

Schirmer et al. (2007) analyze a total of $\sim 20 \text{ deg}^2$ data collected from different observations with different observational depth. They present a sample of shear-selected clusters containing total 158 candidates identified by two types of statistics. Using only S -statistics which is similar to the aperture mass statistics but with different filtering functions, they find 91 peaks with significance being higher than 4. Among them, there are 48 dark ones without obvious optical counterparts. It is found that the fraction of dark peaks is relatively high in shallow surveys with low surface number density of source galaxies. This indicates that a significant number of dark peaks could be false ones resulting from intrinsic ellipticities. Since their filtering functions are complicated with different filtering scales, we cannot do quantitative analyses on the constraints on intrinsic alignments with these dark peaks. However, we may give some rough estimates. In Schirmer et al. (2007), the filtering scales used in peak identifications range from $1.6'$ to $19.8'$ with most of them being larger than $2'$. Comparing the functional form of the Gaussian smoothing with the filtering functions used in Schirmer et al. (2007), their filtering should have the effects corresponding to Gaussian smoothings with $\theta_G \geq 1'$. Thus we use the results of $\theta_G = 1'$ for a conservative discussion. Without intrinsic alignments, our results show that the average number of false peaks in 20 deg^2 with $\nu_{ran} \geq 4$ is about 6. The existence of intrinsic alignments enhances the average number of false peaks. If the 48 dark peaks are all false ones and the number is $+1\sigma$ from the average number of false peaks, we need the average number to be $N_{peak} \sim 42$. Then we have to have $\sigma_{0corr}^2/\sigma_{0ran}^2 \sim 35\%$ to get such a high number of false peaks. For the redshift distribution of source galaxies, Schirmer et al. (2007) give $\alpha = 2$, $\beta = 1.5$ and $z_s = 0.4$ for shallow surveys. The surface number density is $n_g \sim 12 \text{ arcmin}^{-2}$, and $\sigma_\epsilon \sim 0.48$ (Schirmer et al. 2007). We then estimate $\sigma_{0ran}^2 \sim 0.0015$. Thus the ratio $\sigma_{0corr}^2/\sigma_{0ran}^2 \sim 35\%$ requires the parameter A to be $A \sim 32$, which is much higher than the constraint $A \leq 1.29$ from SDSS. Therefore it is very unlikely that the 48 dark peaks are all false ones from intrinsic ellipticities of background galaxies. As we discussed previously and also in Schirmer et al. (2007), the joint effects of small mass clumps and the intrinsic ellipticities could contribute significantly to the number of dark peaks with high significance. It should be pointed out that the functional form and the scale of the filtering function adopted by Schirmer et al.

(2007) are optimized to detect clusters with NFW density profiles. With Gaussian smoothings, the number of peaks and their properties may change quantitatively. It is therefore desirable to analyze the observations with Gaussian smoothings so that we can perform detailed analyses on the statistics of false peaks. On the other hand, it is also worthwhile investigating the noise properties and the associated statistics of false peaks under different smoothing schemes. As the catalog of Schirmer et al. (2007) is the largest one so far, from many aspects careful observational and theoretical studies on these dark peaks are highly valuable.

Future surveys with larger areas will result many more peaks. If a large number of false peaks from intrinsic ellipticities can be securely identified, we can put tight constraints on the level of intrinsic alignments. Considering Poisson fluctuations, we can estimate, as follows, how well the quantity $x = \sigma_{0corr}^2/\sigma_{0ran}^2$ can be constrained from N false peaks with $\nu_{ran} \geq \nu_0$. With the average cumulative number of peaks $N_{peak} \propto \nu \exp(-\nu^2/2)$ for $\nu \geq 3$, where ν is the true significance (e.g., van Waerbeke 2000), we have, for the central value of x , denoted by x_c ,

$$N_{ran} \frac{(\nu_0/\sqrt{1+x_c}) \exp[-\nu_0^2/2/(1+x_c)]}{\nu_0 \exp[-\nu_0^2/2]} = \frac{N_{ran}}{\sqrt{1+x_c}} \exp\left[\frac{\nu_0^2 x_c}{2(1+x_c)}\right] = N, \quad (31)$$

where N_{ran} is the average number of false peaks expected in the field without considering intrinsic alignments. The $\pm 1\sigma$ constraints on x can then be obtained by

$$\frac{N_{ran}}{\sqrt{1+x_c+\delta x}} \exp\left[\frac{\nu_0^2(x_c+\delta x)}{2(1+x_c+\delta x)}\right] - \sqrt{\frac{N_{ran}}{\sqrt{1+x_c+\delta x}} \exp\left[\frac{\nu_0^2(x_c+\delta x)}{2(1+x_c+\delta x)}\right]} = N, \quad (32)$$

and

$$\frac{N_{ran}}{\sqrt{1+x_c-\delta x}} \exp\left[\frac{\nu_0^2(x_c-\delta x)}{2(1+x_c-\delta x)}\right] + \sqrt{\frac{N_{ran}}{\sqrt{1+x_c-\delta x}} \exp\left[\frac{\nu_0^2(x_c-\delta x)}{2(1+x_c-\delta x)}\right]} = N. \quad (33)$$

With $\delta x \ll 1$, we have

$$\delta x \approx \frac{1}{\nu_0^2/2 - 1/2} \frac{\sqrt{N}}{N} \frac{1}{1 + 0.5/\sqrt{N}}. \quad (34)$$

For instance, with $N = 50$ and $\nu_0 = 4$, we have $\delta x \sim 1.8\%$, i.e., the quantity x can be constrained to the level of $x_c \pm 1.8\%$ (1σ). From δx to $\delta(\sigma_{0corr}^2)$, it depends on σ_{0ran}^2 , and thus on n_g and σ_ϵ . Further from the constraint on σ_{0corr}^2 to the constraint on A , we need the redshift distribution of background galaxies. With $n_g = 30 \text{ arcmin}^{-2}$, $\sigma_\epsilon = 0.4$, $\alpha = 2$, $\beta = 1.5$, and $z_s = 0.7$, we have $\delta(\sigma_{0corr}^2) \sim 7 \times 10^{-6}$, and $\delta(A) \sim 0.9$. From the relation between $2\sigma_{0corr}^2$ and the intrinsic alignment $C_{11} + C_{22}$ smoothed over the angular scale θ_G , the limit $\delta(\sigma_{0corr}^2) \sim 7 \times 10^{-6}$ leads to $\delta(C_{11} + C_{22}) \sim 1.4 \times 10^{-5}$ over $\theta_G = 1'$.

Intrinsic alignments of galaxies have been estimated from nearby surveys SuperCOSMOS (Brown et al. 2002) and SDSS (Mandelbaum et al. 2006) assuming negligible lensing effects. Extrapolating their results to redshifts $z \sim 1$ appropriate for most lensing surveys suffers many uncertainties (Brown et al. 2002; Mandelbaum et al. 2006). Heymans et al. (2004) estimated the intrinsic alignments in the COMBO-17 survey ($z \sim 0.6$) from close pairs of background galaxies. Their error bar at ~ 1 arcmin is about *a few* $\times 10^{-4}$. Our above analysis based on only 5 false peaks already gives rise to a tighter constraint on the order of $\delta(C_{11} + C_{22}) \sim 4 \times 10^{-5}$, demonstrating the great potential of our proposed method.

5. Discussion

In this paper, we investigate the effect of the intrinsic alignments of background galaxies on weak lensing detections of mass concentrations. Focusing on the convergence κ -maps, we analyze the number of false peaks due to the intrinsic ellipticities of background galaxies taking into account their intrinsic alignments. Under the assumption of Gaussianity for the noise field, the number of false peaks in κ maps depends on two characteristic parameters γ_p and θ_* , which are in turn determined by the two-point correlations of the field. Without intrinsic alignments, $\gamma_p = \sqrt{2}/2$ and $\theta_* = (\sqrt{2}/2)\theta_G$ for a Gaussian window. Thus the number of false peaks in terms of $\nu_{ran} = N/\sigma_{0ran}$ does not depend on σ_{0ran} (Note that given ν_{ran} , the strength of a peak N depends on σ_{0ran}). With the intrinsic alignments, however, both γ_p and θ_* change with σ_{0corr} . More importantly, the full noise variance $\sigma_0^2 = \sigma_{0ran}^2 + \sigma_{0corr}^2$ cannot be measured easily in real observations. Only the quantity σ_{0ran}^2 can be estimated. Therefore observationally defined signal-to-noise ratio is often with respect to σ_{0ran} rather than to the true noise variance σ_0 . For a given ν_{ran} , the true signal-to-noise ratio ν decreases with the increase of σ_{0corr} . Because $N_{peak}(\nu)$ drops steeply at large ν , the cumulative number of false peaks given a threshold on ν_{ran} increases sensitively as σ_{0corr} increases. This can result a large reduction of the efficiency of weak lensing cluster detections. If a 75% efficiency is expected in the case $\sigma_{0corr} = 0$ for a survey at a detection threshold $\nu_{ran} = 3.5$, this number goes down to 65% with $\sigma_{0corr}^2 \approx 0.1\sigma_{0ran}^2$. The increase of the number of false peaks with intrinsic alignments can also affect the statistical likelihood in judging whether a dark peak truly corresponds to a dark clump or is a false one from intrinsic ellipticities of source galaxies.

On the other hand, the number of false peaks can be a sensitive probe to the intrinsic alignments of background galaxies. A value $\sigma_{0corr}^2 \approx 0.1\sigma_{0ran}^2$ results $N_{peak}(\nu_{ran} \geq 3.5, \sigma_{0corr}) = 1.7N_{peak}(\nu_{ran} \geq 3.5, \sigma_{0corr} = 0)$. Thus it is easier to derive information of σ_{0corr}^2 from $N_{peak}(\nu_{ran})$ than to directly measure σ_{0corr}^2 from two-point correlations. The studies

of CFHTLS Deep cluster survey find that 5 out of 14 peaks with $\nu_{ran} > 3.5$ in the area of 3.61 deg^2 are possibly false ones. We then obtain a constraint $\sigma_{0corr}^2 < 2 \times 10^{-5} (1\sigma)$, which corresponds to the constraint on A in eq. (4) with $A < 2.9$, fully consistent with the limit from SDSS observations. Future large surveys can generate samples containing many lensing detected candidates. If one can find 50 false peaks, the quantity $\sigma_{0corr}^2/\sigma_{0ran}^2$ can be constrained to $\delta(\sigma_{0corr}^2/\sigma_{0ran}^2) \sim 1.8\%$. With $\sigma_{0ran}^2 \sim 4 \times 10^{-4}$, we then have $\delta(\sigma_{0corr}^2) \sim 7 \times 10^{-6}$ and $\delta(C_{11} + C_{22}) \sim 1.4 \times 10^{-5}$.

The intrinsic alignments of galaxies carry important information of galaxy formation, especially the environmental effects. Previous observational studies show that the intrinsic alignments of galaxies are at the lower end of the theoretical predictions for dark matter halos, indicating the possible existence of misalignment between galaxies and their host halos (e.g., Heymans et al. 2006). The method proposed in this paper allows us to constrain the intrinsic alignments of galaxies to a very high precision, and therefore is very promising in detailed studies on the formation of galaxies.

In our analysis, we assume a Gaussian statistics for the noise in smoothed κ fields for both cases with or without intrinsic alignments. Although we do not expect a highly non-Gaussian smoothed noise field because of the central limit theorem, its detailed statistical properties deserve thorough investigations. The existence of intrinsic ellipticities as well as their alignments not only produces false peaks in κ maps, but also affects the height of the true peaks that are associated with clusters of galaxies. From previous discussions, we have $K_N(\vec{\theta}) = K(\vec{\theta}) + N(\vec{\theta})$ for smoothed κ fields. Assuming that K and N are independent of each other, we can write the distribution of K_N in the form $p(K_N)dK_N = [\int p_K(K)p_N(K_N - K)dK]dK_N$. It is seen that $p(K_N)$ depends on the statistics of K and N . Thus detailed analyses on the statistical properties of K and N are crucial in order to understand how the true peaks are influenced by the noise. Further complications arise due to the shear-ellipticity correlations (e.g., Hirata & Seljak 2004; Mandelbaum et al. 2006). Because the ellipticities of galaxies are associated with the properties of their host halos, correlations between the ellipticities of foreground galaxies and the shears generated by their host halos on background galaxies are expected. Then K and N are not independent quantities anymore. The effects of intrinsic alignments and shear-ellipticity correlations on lensing analyses depend differently on the redshift distribution of background galaxies. The narrower the distribution is, the stronger the effects of the intrinsic alignments are. For shear-ellipticity correlations, the effects are stronger for broader distributions. For tomographic lensing studies, the intrinsic alignments are important for galaxies within the same redshift bins, while the shear-ellipticity correlations are significant in considering the cross correlations between different bins. Extensive investigations on these problems and their effects on weak lensing cluster surveys will be pursued in our future research.

Weak lensing cluster studies together with other lensing analyses are sensitive probes of the dark matter distribution as well as the nature of dark energy (e.g., Fang & Haiman 2006). With fast observational advances and thorough theoretical understandings of different systematics, cosmological applications of weak lensing effects will greatly improve our knowledge about the universe.

We sincerely thank the referee for the encouraging and constructive comments and suggestions. This research was supported in part by the National Science Foundation of China under grants 10243006 and 10373001, by the Ministry of Science and Technology of China under grant TG1999075401, by the Key Grant Project of Chinese Ministry of Education (No. 305001), and by the National Science Foundation of China under grant 10533010.

REFERENCES

- Bartelmann, M., & Schneider, P. 2001, *Physics Reports*, 340, 291
- Bode, P., Ostriker, J. P., Weller, J., & Shaw, L. astro-ph/0612663
- Bond, J. R., & Efstathiou, G. 1987, *MNRAS*, 226, 655
- Borgani, S. 2006, astro-ph/0605575
- Brown, M. L., Taylor, A. N., Hambly, N. C., & Dye, S. 2002, *MNRAS*, 333, 501
- Croft, R. A. C., & Metzler, C. A. 2000, *ApJ*, 545, 561
- Crittenden, R. G., Natarajan, P., Pen, U. L., & Theuns, T. 2001, *ApJ*, 559, 552
- Erben, Th., van Waerbeke, L., Mellier, Y., Schneider, P., Cuillandei, J. C., Castander, F. J. & Dantel-Fort, M. 2000, *A&A*, 355, 23
- Fang, W., & Haiman, Z. 2006, astro-ph/0612187
- Gavazzi, R., & Soucail, G. 2007, *A&A*, 462, 259
- Hamana, T., Takada, M., & Yoshida, N. 2004, *MNRAS*, 350, 893
- Heavens, A., Refregier, A., & Heymans, C. 2000, *MNRAS*, 319, 649
- Hennawi, J. F. & Spergel, D. N. 2005, *ApJ*, 624, 59

- Heymans, C., Brown, M., Heavens, A., Meisenheimer, K. Taylor, A., & Wolf, C. 2004, MNRAS, 347, 895
- Heymans, C., White, M., Heavens, A., Vale, C., & van Waerbeke, L. 2006, MNRAS, 371, 750
- Hirata, C. M., & Seljak, U. 2004, Phys. Rev. D., 70, 063526
- Hoekstra, H., Mellier, Y., van Waerbeke, L., Semboloni, E., Fu, L., Hudson, M. J., Parker, L. C., Tereno, I., & Benabed, K. 2006, ApJ, 647, 116
- Jing, Y. P. 2002, MNRAS, 335, L89
- Kaiser, N., & Squires, G. 1993, ApJ, 404 441
- King, L. J., & Schneider, P. 2003, A&A, 398, 23
- King, L. J. 2006, A&A, 441, 47
- Knox, L. , Song, Y., & Tyson, J. A. 2006, Phys. Rev. D., 74, 023512
- von der Linden, A., Erben, T., Schneider, P., & Castander, F. J. 2006, A&A, 454, 37
- Mandelbaum, R. , Hirata, C. M., Ishak, M., Seljak, U., & Brinkmann, J. 2006, MNRAS, 367, 611
- Massey, R. et al. 2007, Nature, 445, 286
- Munshi, D. , Valageas, P., van Waerbeke, L., & Heavens, A. 2006, astro-ph/0612667
- Navarro, J., Frenk, C. & White, S. D. M. 1996, ApJ, 462, 563
- Porciani, C. , Dekel, A., & Hoffman, Y. 2002, MNRAS, 332, 32
- Semboloni, E., van Waerbeke, L., Heymans, C., Hamana, T., Colombi, S., White, M., & Mellier, Y. 2007, MNRAS, 375L, 6
- Schirmer, M., Erben, T., Hettterscheidt, M., & Schneider, P. 2007, A& A, 462, 875
- Schneider, P. 1996, MNRAS, 283, 837
- Starck, J. L., Pires, S. & Refregier, A. 2006, A& A, 451, 1139
- Tang, J. Y., & Fan, Z. H. 2005, ApJ, 635, 60
- van Waerbeke, L. 2000, MNRAS, 313, 524

White, M., van Waerbeke, L., & Mackey, J. 2002, ApJ, 575, 640

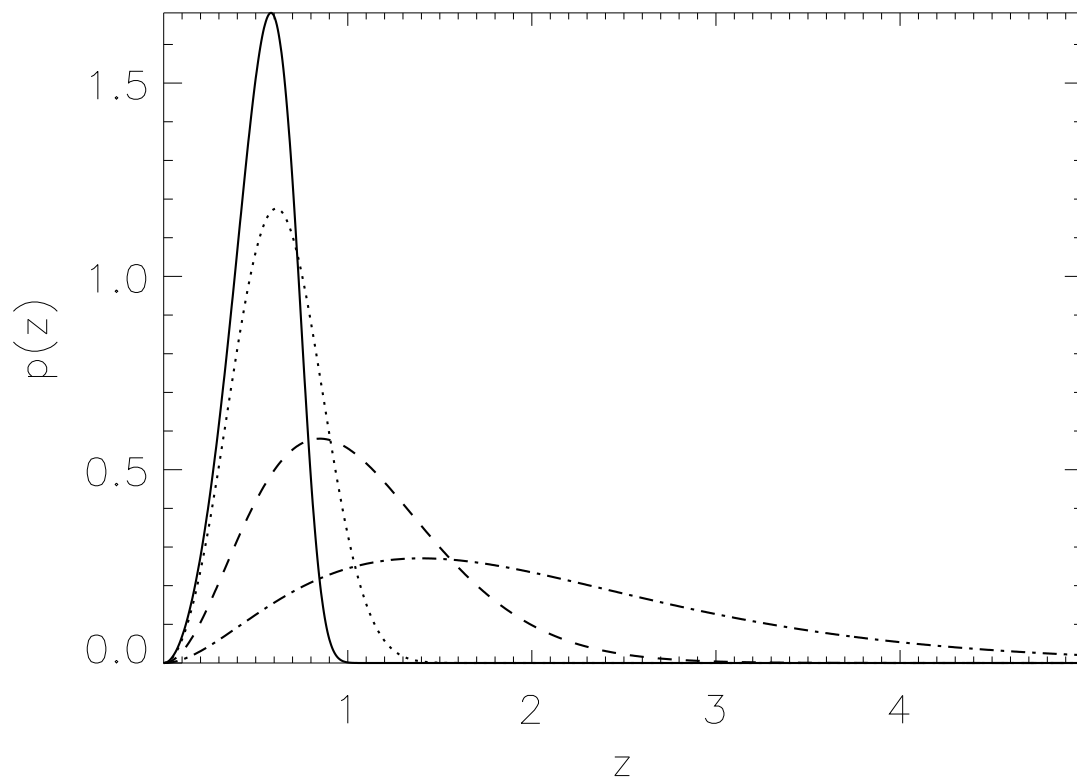


Fig. 1.— The redshift distribution of background galaxies with the functional form given in eq. (24). Here we take $\alpha = 2$ and $z_s = 0.7$. The solid, dotted, dashed, and dash-dotted lines correspond to $\beta = 6, 3, 1.5$ and 1 , respectively.

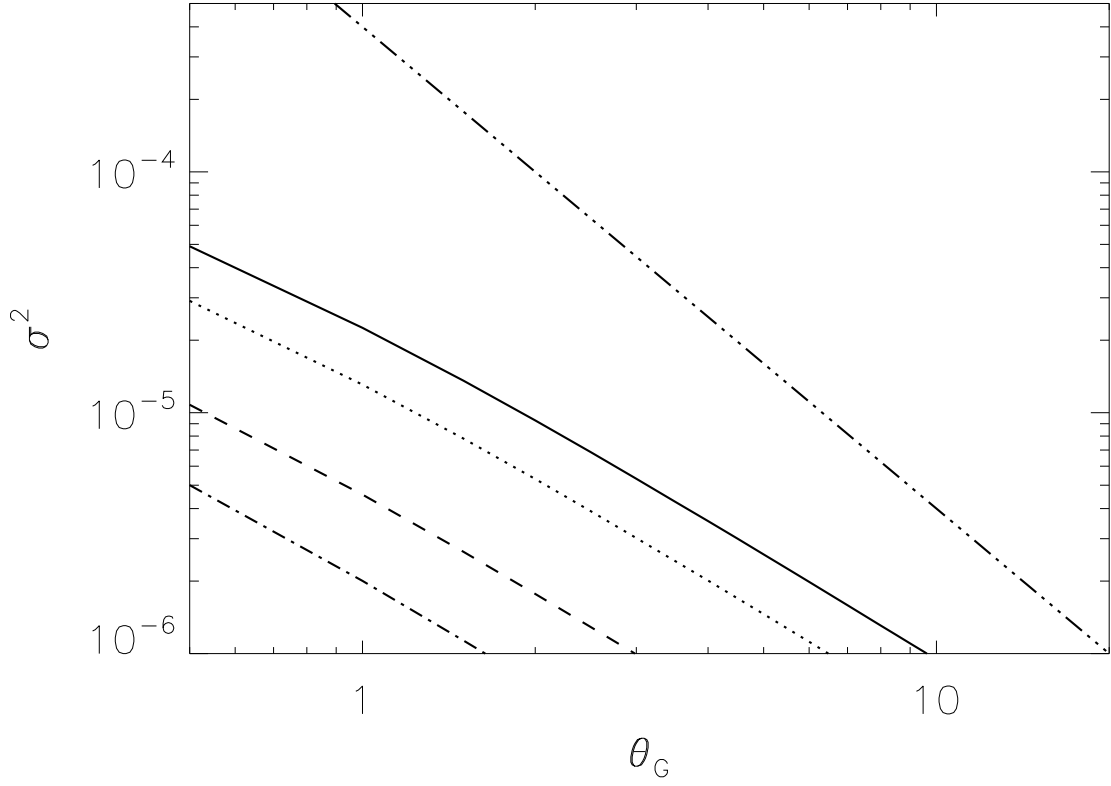


Fig. 2.— The variance contributed by intrinsic alignments. We take $A = 0.57$ in eq. (4), and $\alpha = 2$ and $z_s = 0.7$ in eq. (24). The solid, dotted, dashed, and dash-dotted lines correspond to the results with $\beta = 6, 3, 1.5$ and 1, respectively. The dash-dot-dot-dotted line is σ_{0ran}^2 with $\sigma_\epsilon = 0.4$ and $n_g = 30 \text{ arcmin}^{-2}$.

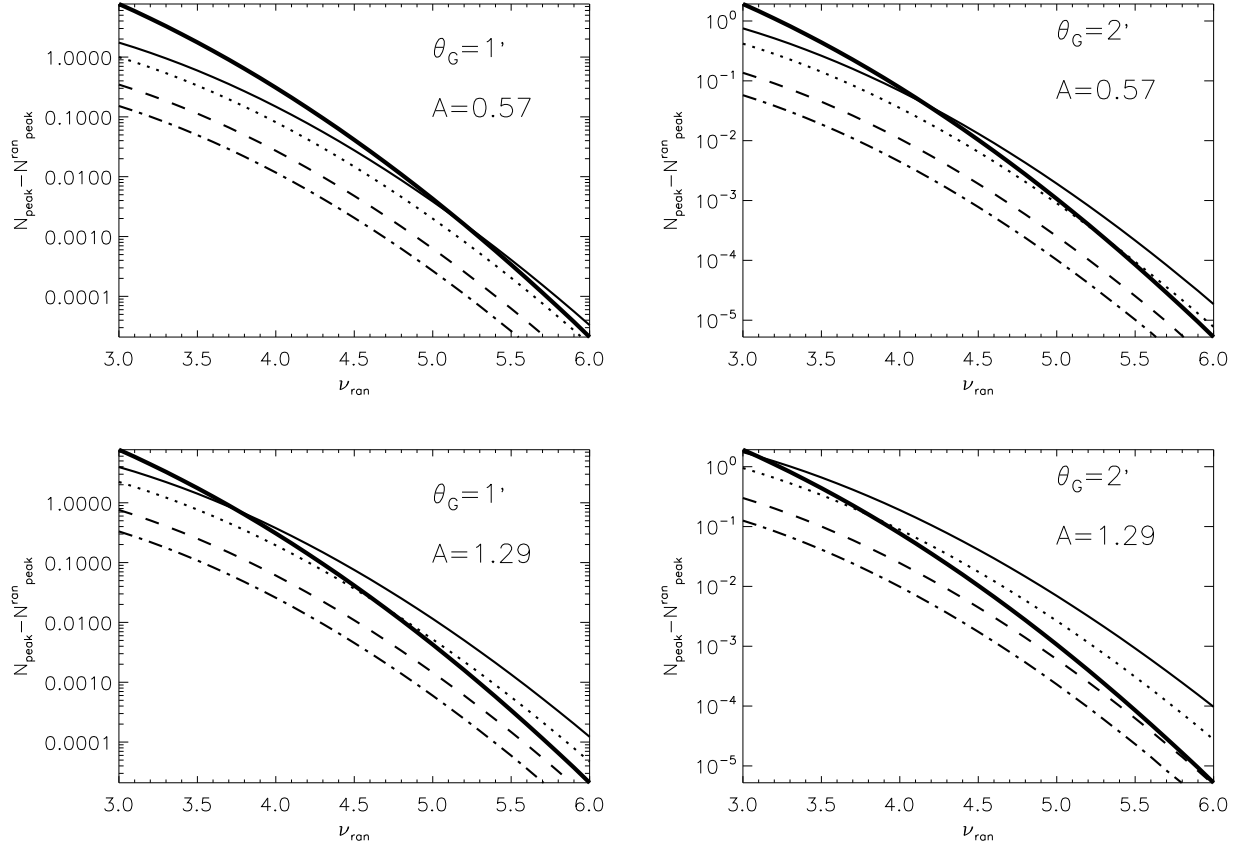


Fig. 3.— The cumulative number of false peaks resulting from intrinsic alignments in 1 deg^2 . The thick solid line is the cumulative number of false peaks without intrinsic alignment. The thin solid, dotted, dashed, and dash-dotted lines are for $\beta = 6, 3, 1.5$, and 1 , respectively.

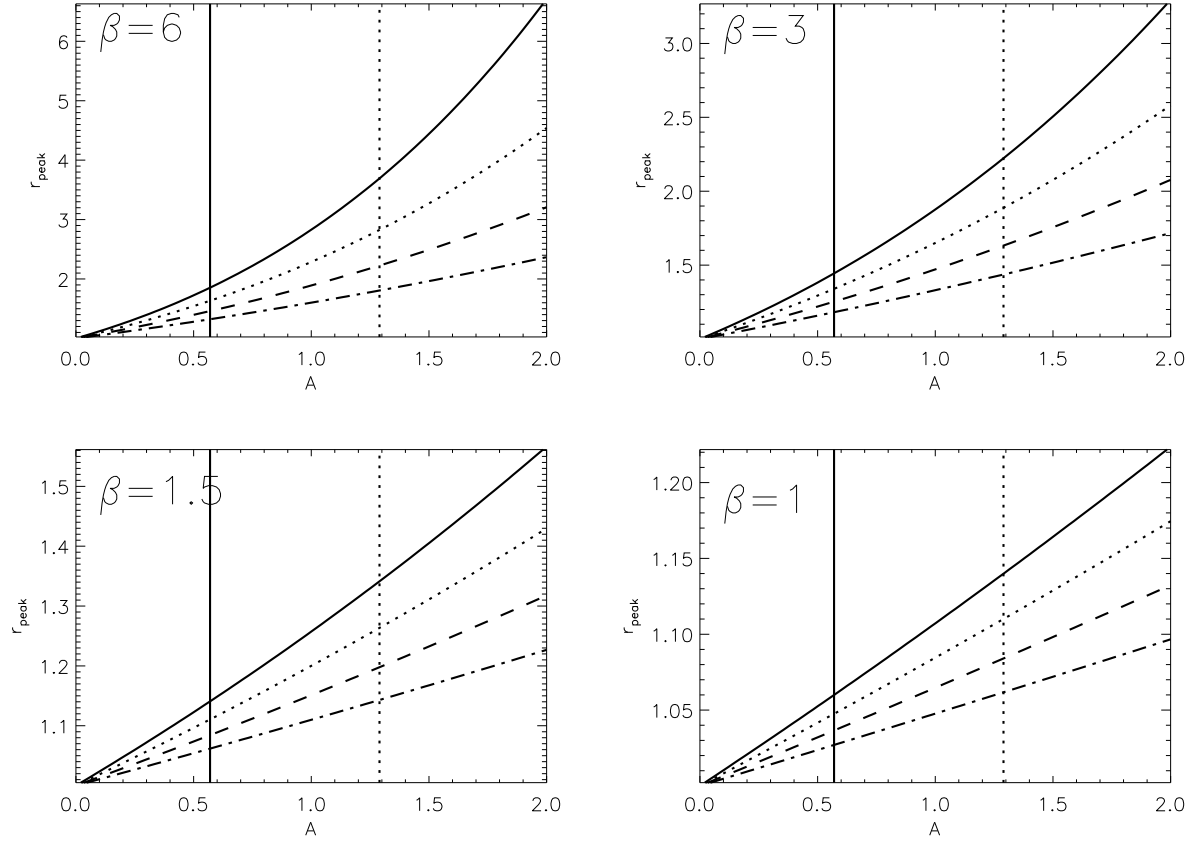


Fig. 4.— The dependence of the ratio $r_{\text{peak}} = N_{\text{peak}}/N_{\text{peak}}^{\text{ran}}$ on A for $\theta_G = 1$ arcmin. Different panels show the results with different β values. The solid, dotted, dashed, and dash-dotted lines are for $\nu_{\text{ran}} = 5, 4.5, 4$, and 3.5 , respectively. The solid and dotted vertical lines are respectively at the position of $A = 0.57$ and $A = 1.29$.

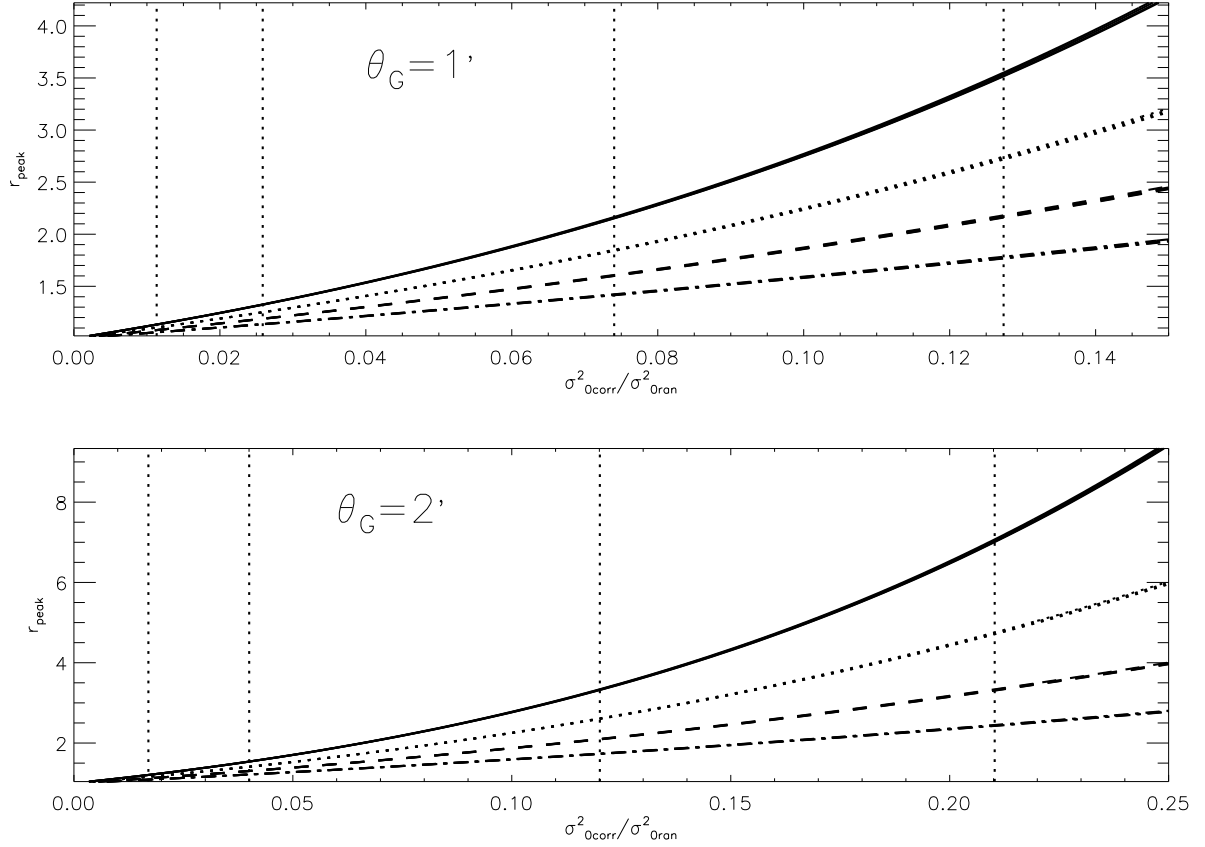


Fig. 5.— The ratio r_{peak} with respect to $\sigma^2_{0corr}/\sigma^2_{0ran}$. The upper and lower panels correspond to $\theta_G = 1$ arcmin and $\theta_G = 2$ arcmin, respectively. The four sets of solid, dotted, dashed and dash-dotted lines are respectively for $\nu_{ran} = 5, 4.5, 4$, and 3.5 . Each set of lines contains results with $\beta = 6, 3, 1.5$ and 1 . The vertical dotted lines from right to left show the value of $\sigma^2_{0corr}/\sigma^2_{0ran}$ with $A = 1.29$ for $\beta = 6, 3, 1.5$ and 1 , respectively.

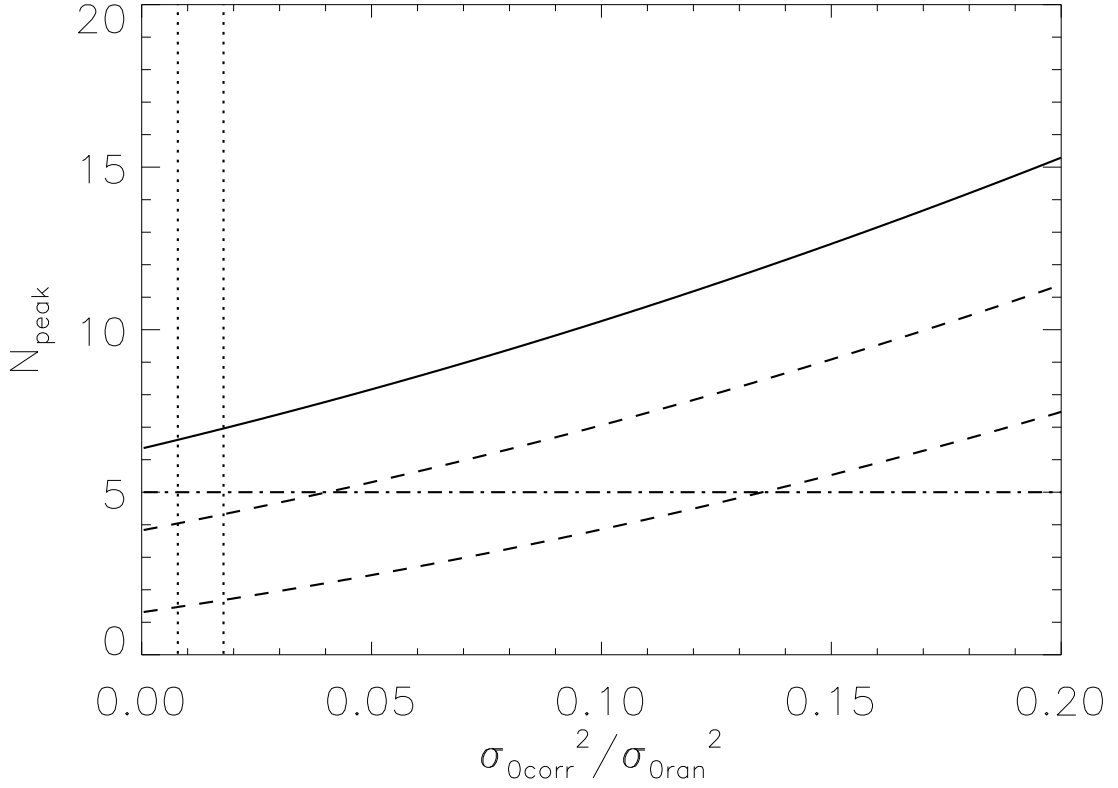


Fig. 6.— The number of false peaks with $\nu_{ran} \geq 3.5$ in 3.61 deg^2 . The solid line is for the average number of false peaks. The upper and lower dashed lines represent -1σ and -2σ Poisson deviations from the mean, respectively. The horizontal dash-dotted line is at $N_{peak} = 5$. The two vertical dotted lines correspond to the values of $\sigma_{0corr}^2 / \sigma_{0ran}^2$ for the CFHTLS Deep with $A = 0.57$ and $A = 1.29$, from left to right, respectively.

Table 1: Ratio of $\sigma_{0corr}^2/\sigma_{0ran}^2$ with $\alpha = 2$, $z_s = 0.7$, $n_g = 30 \text{ arcmin}^{-2}$ and $\sigma_\epsilon = 0.4$

β	z_{med}	$\sigma_{0corr}^2/\sigma_{0ran}^2$ ($\theta_G = 1'$) ($A = 0.57$)	$\sigma_{0corr}^2/\sigma_{0ran}^2$ ($\theta_G = 2'$) ($A = 0.57$)	$\sigma_{0corr}^2/\sigma_{0ran}^2$ ($\theta_G = 1'$) ($A = 1.29$)	$\sigma_{0corr}^2/\sigma_{0ran}^2$ ($\theta_G = 2'$) ($A = 1.29$)
6	0.55	6%	10%	13.5%	22.6%
3	0.62	3%	5%	6.8%	11.3%
1.5	0.99	1%	2%	2.3%	4.5%
1	1.87	0.5%	0.8%	1.1%	1.8%

Table 2: Ratio of $\sigma_{0corr}^2/\sigma_{0ran}^2$ for different surveys. For the redshift distribution, we take $\alpha = 2$ and $\beta = 1.5$.

	$\langle z \rangle$	z_s	z_{med}	n_g (arcmin^{-2})	$\sigma_{0corr}^2/\sigma_{0ran}^2$ ($\theta_G = 1'$) ($A = 0.57$)	$\sigma_{0corr}^2/\sigma_{0ran}^2$ ($\theta_G = 2'$) ($A = 0.57$)
COSMOS	1.2	0.8	1.13	70	2.3%	3.5%
SNAP	1.2	0.8	1.13	100	3.3%	5%
SNAP(Deep)	1.4	0.93	1.3	300	8.4%	12.8%

Table 3: Probability for the detected clumps being false peaks from chance alignments of background galaxies. Here n_{clump} denotes the number of clumps found in the field, $p(ran)$ represents the probability without intrinsic alignments, and $p(corr)$ is the probability taking into account intrinsic alignments with $A = 1.29$.

Obs.	Area deg ²	n_g (arcmin ⁻²)	θ_G (arcmin)	ν_{ran}	n_{clump}	$p(ran)$	$p(corr)$
Erben et al. (2000)	0.05	20	0.5	4.5	1	0.9%	1%
Linden et al. (2006)	0.05	65	0.5	3	1	30%	27%
Massey et al. (2007)	2	70	1	4	2	10%	15%
Massey et al. (2007)	2	70	1	4.5	2	0.3%	0.6%
Massey et al. (2007)	2	70	1	5	2	0.003%	0.01%